Bull Volcanol (1986) 48: 127–141

Bulletin of
Volcanology

© Springer-Verlag 1986

The 1982 eruptions of El Chichon volcano, Mexico (2): Observations and numerical modelling of tephra-fall distribution

Steven Carey and Haraldur Sigurdsson

Graduate School of Oceanography, University of Rhode Island, Kingston, RI 02881, USA

Abstract. Tephra fallout from the A-1 (March 29, 0532 UT), B (April 4, 0135 UT), and C (April 4, 1122 UT) 1982 explosive eruptions of El Chichon produced three tephra fall deposits over southeastern Mexico. Bidirectional spreading of eruption plumes, as documented by satellite images, was due to a combination of tropospheric and stratospheric transport, with heaviest deposition of tephra from the ENE tropospheric lobes. Maximum column heights for the eruptions of 27, 32, and 29 km, respectively, have been determined by comparing maximum lithic-clast dispersal in the deposits with predicted lithic isopleths based on a theoretical model of pyroclast fallout from eruption columns. These column heights suggest peak mass eruption rates of 1.1×10^8, 1.9×10^8, and 1.3×10^8 kg/s. Maximum column heights and mass eruption rates occured early in each event based on the normal size grading of the fall deposits. Sequential satellite images of plume transport and the production of a large stratospheric aerosol plume indicate that the eruption columns were sustained at stratospheric altitudes for a significant portion of their duration. New estimates of tephra fall volume based on integration of isopach area and thickness yield a total volume of 2.19 km^3 (1.09 km^3 DRE, dense rock equivalent) or roughly twice the amount of the deposit mapped on the ground. Up to one-half of the erupted mass was therefore deposited elsewhere as highly dispersed tephra.

Introduction

El Chichon volcano, in the state of Chiapas, southeastern Mexico, erupted explosively on March 29, 1982, ending a repose period of 550 years (Tilling et al. 1984; Duffield et al. 1984). Following one month of intense shallow seismic activity at about 5 km depth (Havskov et al. 1983), three major eruptions and numerous minor phreatic events occured between March 29 and April 4. The three major eruptions occurred on March 29 (0532 UT), April 4 (0135 UT), and April 4 (1122 UT) and have been designated as the A-1, B, and C eruptions, respectively (Sigurdsson et al. 1984; Varekamp et al. 1984). The major eruptions produced widespread tephra fallout and generated devastating pyroclastic surges and flows (Sigurdsson et al. 1984). Nine villages within a roughly 7 km radius of the volcano were partially or completely destroyed by surges, and as many as 2000 people may have lost their lives.

Much attention has been focused on the massive injection of sulfur, as SO_2, into the stratosphere and the potential for climatic modification (e.g., Pollack et al. 1982; Luther and MacCracken 1982). The unusually high sulfur content of the 1982 magma remains an enigma (Luhr et al. 1984; Rye et al. 1984), yet promises to greatly increase our understanding of the role of sulfur-rich eruptions in climatic oscillations (Devine et al. 1984; Rampino and Self 1982). Geochemical studies indicate that the preeruption magmatic sulfur content may have been as high as 2.3 wt % (SO_3) (Varekamp et al. 1984; Devine et al. 1984). Such high contents of sulfur relative to the other, typically dominant, volatile constituents, such as H_2O and CO_2, suggests that sulfur may have played a significant role in the eruptions (Carey and Sigurdsson, in preparation).

In another paper, we have documented the stratigraphy of the pyroclastic deposits from the 1982 eruptions of El Chichon and presented a model for the evolution of eruptive processes (Sigurdsson et al. 1984). In this paper we focus on the grain size distributions, isopleth and isopach geometries of tephra-fall deposits from the three major 1982 eruptions and relate them to variations in eruption column dynamics and atmo-

Offprint requests to: S Carey

spheric transport by using information from satellite imagery and a computer model of tephra fallout.

Satellite observations of eruption plumes

Dispersal of plumes from the three major eruptions was recorded by the GOES-East weather satellite using both IR and visible-band imagery (Ness 1982; Matson 1984). Each event was characterized by plume dispersal in two principal directions: east-northeast and south-southwest (Fig. 1). Radiosonde profiles from the meteorological stations at Veracruz and Merida (380 and 590 km northwest and northeast of El Chichon, respectively) show that ENE transport was controlled by tropospheric winds, extending up to 18 km in altitude, whereas WSW transport was the result of stratospheric winds above 18 km (Fig. 2). The differential transport produced elongate plumes which initially expanded symmetrically along a ENE-WSW axis. The ENE lobes of the plumes show consistently higher velocities in the latter stages of each eruption relative to the WSW lobes. This is most likely the result of slightly higher velocity tropospheric winds over the Yucatan Pennisula, as shown by the radiosonde data from Merida and Veracruz (Fig. 2).

The average velocities of plume fronts (ENE and WSW lobes) for the A-1, B, and C eruptions were determined from sequential GOES-East weather satellite images (Table 1). Plume front velocities of the ENE

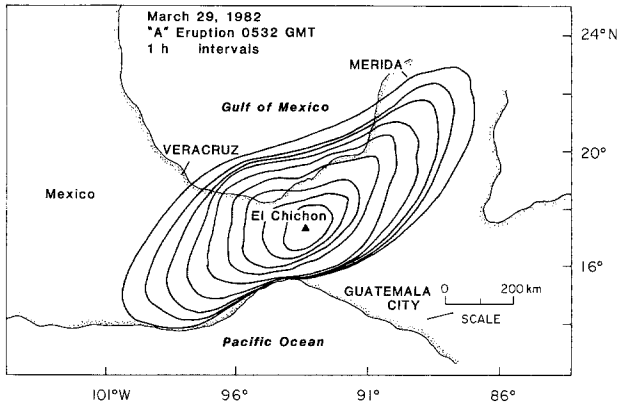

Fig. 1. Lateral growth of the March 29, 1982 (A-1) eruption cloud from El Chichon volcano as recorded by the GOES weather satellite. Contours are in one hour intervals. Bi directional spreading is due to a combination of tropospheric (ENE) and stratospheric (WSW) transport

lobes for the A-1 and C eruptions are in good agreement with observed tropospheric winds. Available velocity data for the B eruption are, on the other hand, restricted to the first two hours of the event because of an incomplete sequence of satellite photographs. During the first hour all three of the major events have plume front velocities which are up to 70% greater than the local tropospheric winds. The high initial velocities can be attributed to the forced intrusion of the plume into the atmosphere, resulting in large lateral velocities.

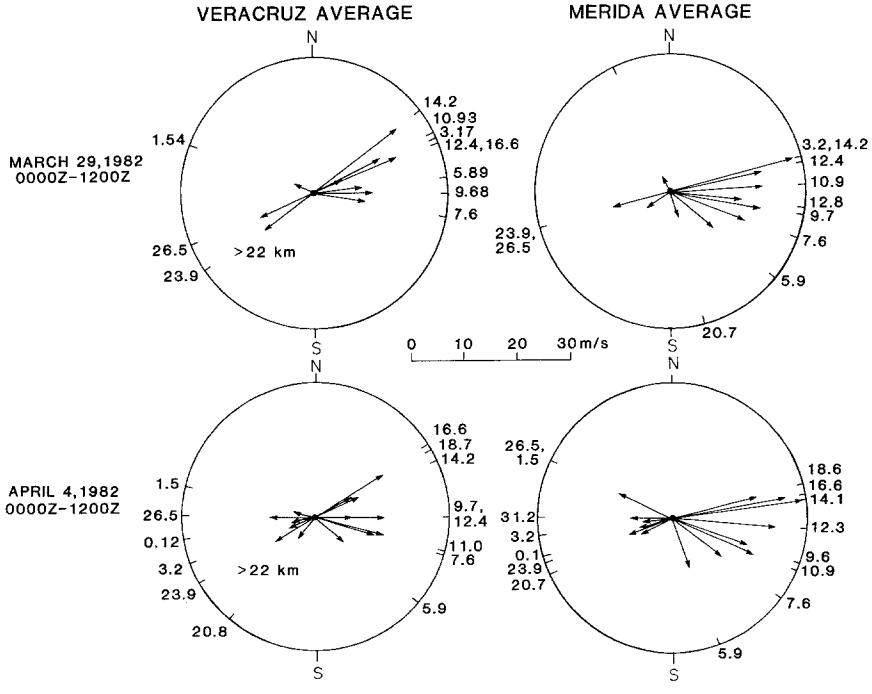

Fig. 2. Average wind-velocity profiles at Veracruz and Merida for March 29, 1982 (0000Z–1200Z), and April 4, 1982 (0000Z–1200Z), calculated from radiosonde soundings. Wind vectors point in the direction to which the wind is blowing and the lengths are proportional to the magnitude of the wind (see scale in center of diagram). Corresponding elevations in km are given around the circumference of each circle

Table 1. Plume-front velocities and horizontal expansions

Eruption	A-1	B	C
ENE lobe			
Ave. vel. (m/s)[a]	21 (9 h)	44 (2 h)	30 (7 h)
Max. tropo. wind vel. (m/s)[a]	26 (M)	26 (M)	28 (M)
WSW lobe			
Ave. vel. (m/s)	19 (9 h)	21 (2 h)	19 (7 h)
Max. strato. wind vel. (m/s)	20 (GC)	10 (M)	10 (M)
Horizontal expansion[b] (km^2/s)	6.0	11.7	6.0

(M)-Merida radiosonde data
(GC)-Guatemala City radiosonde

[a] Average velocity of the plume front over the period indicated in parentheses, e.g., 9 h
[b] Rate of horizontal plume expansion for the first hour of each eruption

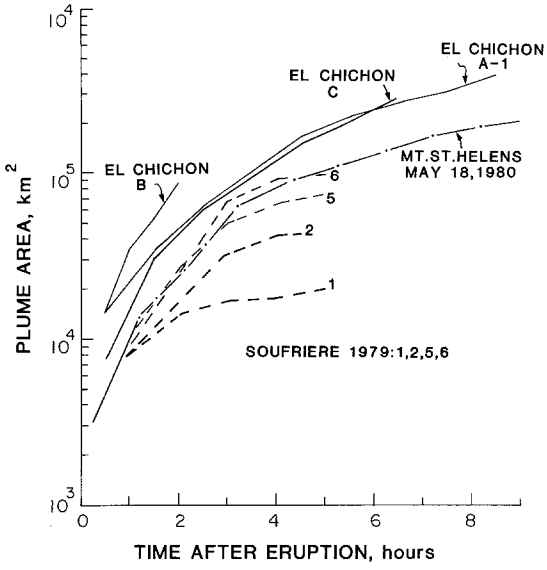

Fig. 3. Eruption plume area (km^2) time for the three major eruptions of El Chichon solid lines; the May 18, 1980 eruption of Mount St. Helens, solid dotted line (data from Sarna-Wojcicki et al. 1981); and four eruptions of the Soufriere, St. Vincent, dashed lines (data from Krueger 1982)

Early horizontal growth of the plume over Mount St. Helens during the May 18, 1980 eruption was in excess of 55 m/s compared to the local maximum tropospheric winds of about 30 m/s (Sarna-Wojcicki et al. 1981; Sparks et al.1986).

The average velocity of the WSW lobe from the A-1 eruption is 19 m/s, in good agreement with the stratospheric wind velocity (Table 1). Unfortunately, stratospheric wind velocities on April 4 are not available from the Guatemala City station. The maximum velocity recorded at the more northern Merida station is only one-half of the dispersal velocity of the WSW lobes (Table 1) and is thus probably not representative of the stratospheric velocities as far south as El Chichon based on the difference recorded between these stations on March 29. It is likely that the velocities on April 4 were comparable to those measured at Guatemala City on March 29. The assignment of WSW-lobe transport to stratospheric altitudes is also supported by the generation of strong gravity waves by eruption columns piercing the tropopause (Mauk 1983) and the production of a stratospheric aerosol layer up to 30 km (Hofmann and Rosen 1983; McCormick and Swissler 1983).

The lateral expansion of each plume with time was also determined from the GOES-East satellite images (Fig. 3, Table 1). The expansion of plumes from the A-1 and C eruptions are similar with initial expansion rates of about 6 km^2/s, which increase to 22 km^2/s after 9 and 7 hours, respectively. At similar time intervals the rate of expansion of both A-1 and C eruption plumes is larger than in the May 18, 1980 eruption of Mount St. Helens (3–10 km^2/s), and plumes from the 1979 eruptions of the Soufriere on St. Vincent (3–9 km^2/s, Fig. 3). Eruption B has the highest intial rate of plume expansion (11.7 km^2/s) of all the El Chichon events (Table 1).

The horizontal expansion of an eruption plume is due to entrainment and thermal expansion of air, wind shear, and diffusion. A buoyant plume rising in a stratified environment such as the atmosphere will spread out between two levels, H_b and H_t. The basal level (H_b) is the altitude at which the plume density is equal to the ambient atmosphere, and the upper level (H_t) is the maximum height attained by the plume as a result of its excess momentum at H_b. Between these levels the plume spreads laterally as a forced intrusion (Sparks 1986). Simple mass balance considerations suggest that the radial velocity is directly proportional to the mass flux at H_b and inversely proportional to the distance from the plume center (Fig. 4). Thus, for eruptions with large mass fluxes, radial velocities between H_b and H_t can easily exceed local wind speeds.

Sparks (1986) has shown that the expansion of the initial Mount St. Helens plume on May 18, 1980, follows a trend predicted by the simple mass balance model (Fig. 4). Data for the growth of the three El Chichon plumes trend at an angle to the predicted curves for various column heights (Fig. 4). Radial velocities were measured perpendicular to the tropospheric and stratospheric lobes in order to elimate the contribution of wind shear. Compared to Mount St. Helens and the predicted curves, the El Chichon events decelerate more rapidly as a function of distance from source. The departure of the El Chichon data from the predicted trends at large radial distance may reflect a decrease in the mass eruption rate with time or

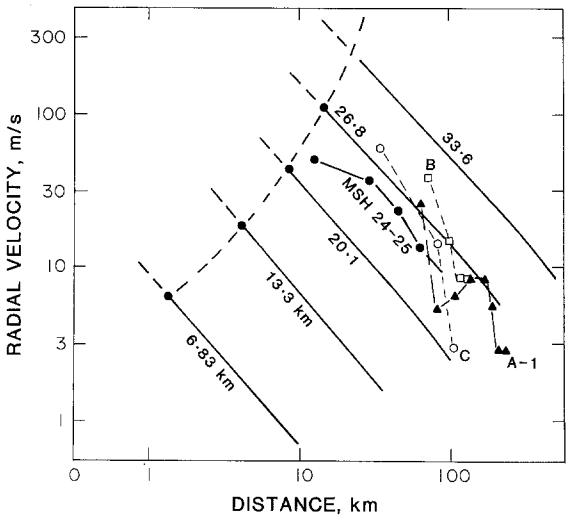

Fig. 4. Change in radial velocity as a function of distance from source for the umbrella regions of eruption columns 6.8–33.6 km in height (solid lines) based on conservation of mass (adapted from Sparks 1986). Solid circles are data from the May 18, 1980 eruption of Mount St. Helens (Sparks et al. 1986). The three eruptions of El Chichon are plotted with open circles (A-1), open squares (B), and solid triangles (C). Dashed curve represents the radius of the column at H_b for various column heights. Radial velocities of the El Chichon plumes were measured perpendicular to the major atmospheric transport directions

alternatively may result from uncertainties in defining the edge of the plume at large distances from source.

The radial velocity data suggest that all of the El Chichon eruption columns were initially in excess of 25 km (Fig. 4). Of the three events, eruption B had the highest initial eruption column and thus the highest mass eruption rate. Eruptions A-1 and C were lower yet comparable to each other in magnitude. Evidence for a larger mass eruption rate during the B eruption is also provided by the greater dispersal of lithics (Sigurdsson et al. 1984) and by the numerical modelling of pyroclast fallout presented later.

The satellite images allow estimates of the duration of each event with the precision of ±0.5 h (Table 2). Eyewitness accounts, seismicity, and satellite images can all be used to define the beginning of each event. On the other hand, the end of each event is more difficult to determine because of the gradual decline in activity and lingering ash clouds which obscure the volcano. We take the end of activity as the onset of significant reduction in plume density and decrease in column height as shown by the IR and visible band satellite images. These are, therefore, maximum estimates for sustained high-altitude column activity but minimum estimates for total eruptive activity. Eruption B was the shortest event of the three main eruptions at 4.5 hours. The longest event was eruption C (7 h), and eruption A-1 was intermediate (6 h).

Distribution and thickness of tephra-fall deposits

Tephra fallout from the three major eruptions of El Chichon affected a large area of southeastern Mexico and part of Guatemala. The area enclosed by the 1.0 mm isopach for the total fall deposit was 4.5×10^4 km^2 prior to compaction and erosion (Varekamp et al. 1984). Deposition occurred primarily from plume lobes transported within the troposphere (< 18 km), as shown by the ENE and E dispersal axis of the deposits (Figs. 5–7). Four widespread tephra-fall layers were produced by the A-1, A-2, B, and C eruptions. Details of the stratigraphy, nature, and distribution of these layers along with associated pyroclastic surges and flows have been presented by Sigurdsson et al. (1984). In this paper we present more detailed isopach and isopleth maps of the tephra-fall deposits which have been updated by field data collected in January 1983. Stratigraphic nomenclature of the fall deposits and their relationship to the 1982 eruptive chronology is presented in Table 2.

The A-1 deposit follows a curved dispersal axis, first trending north, then sweeping to the northeast (Fig. 5). This distribution is most likely the result of tephra transport by both low-altitude N winds (< 4 km) and upper tropospheric NE winds as shown in the March 29 wind profiles (Fig. 2). The layer-B-fallout axis trends east, with a slight S component. This dispersal does not directly match the course of the eruption plume observed from the GOES satellite. The difference between the deposit on the ground and the track of the high altitude plume can be attributed to an increasing southerly component of transport as tephra settled into lower altitude winds (Fig. 2). The orientation of the layer-C-fallout axis is similar to A-1, although not as northerly, which may reflect a dimunition of low altitude winds with a southerly component later in the day of April 4.

The thickest fall deposit within a 25 km radius of the volcano was produced by the A-1 eruption (Fig. 8). Some erosion of tephra-fall deposit B by overlying pyroclastic surges and flows did occur in the proximal area, however, so it is possible that the original thickness of layer B may have exceeded A-1. Thus, our thickness data for layer B within 8 km of the crater are minimum values. The thickness of layer B has a maximum at about 6 km from the crater (Fig. 8). Similar displacements of thickness maxima downwind from source have also been noted for several other deposits (Waitt and Dzurisin 1981; Williams and Self 1983; Sigurdsson et al. 1985; Walker 1980).

Table 2. El Chichon 1982 eruption chronology (All times are GMT)

Date	Eyewitness[a, b]	Satellite[b]	Seismic[a]	Duration (h)	Tephra-fall Designation	Description
March 29	0532	0530–0600	0515	~5	A-1	Major phreatoplinian eruption, eruption column >17 km plume dispersed to the ENE and WSW
March 30	–	1500	–	–	–	Small explosion, plume dispersed to the E about 120 km
March 30	–	2100	–	~4	–	Small explosion, eruption cloud to midtroposhere, plume dispersed 350 km to the N
March 31	–	1930	–	–	–	Small explosion, eruption cloud to upper troposphere, plume dispersed to the E
April 2	1700?	–	–	–	–	Small explosion, mushroom-shaped cloud rose to 3.5 km in 30 min
April 3	–	0000–0030	–	–	–	Small explosion, plume dispersed to the E
April 3'	–	0830–0900	0840	–	A-2	Small eruption, eruption column reached tropopause, plume dispersed to the ENE and WSW
April 3	–	1500	–	–	–	Small explosion, plume dispersed to the SW and SE
April 4	0135	0130–0200	0139	~4	B	Major plinian eruption, eruption column >17 km, plume dispersed to the ENE and WSW, pyroclastic flows and surges
April 4	1122	1130	1110	7	C	Major phreatoplinian eruption, eruption column >17 km, plume dispersed ENE and WSW

[a] Havskov et al. 1983
[b] SEAN Bulletin, vol. 7 no. 3, 1982, and NOAA satellite images (Matson, personal communication)

Grain size and component proportions

The proximal fall deposits can be discriminated on the basis of both grain size and component abundances, as well as stratigraphic position. This is a particularly useful feature where they occur interbedded with thick pyroclastic surges and flows, and the section is only partially exposed (Sigurdsson et al. 1984).

Within 10 km of the crater, the gray, basal, A-1 fall layer is normally graded and consists of juvenile trachyandesitic pumice lapilli, crystals of plagioclase, hornblende, clinopyroxene, Fe-Ti oxides, and predominantly igneous lithic fragments. The overlying A-2 is thin, poorly sorted, and fine grained even in the proximal area, as is typical of falls derived from phreatomagmatic explosions (Self and Sparks 1978). The poor sorting, however, can in part be attributed to impacting and penetration of pyroclasts which fell during the B eruption on the next day. Because of its limited distribution, small volume, and difficulties in obtaining a sample uncontaminated by the B-fall, the A-2 layer will not be discusses further.

The second major fall deposit, layer B, is slightly normally graded, yet quite distinct in appearance from A-1 because of its reddish-gray color, caused by a high content of oxidized and hydrothermally altered lithic fragments. Figure 9 illustrates the difference in component abundances between the fall layers at 6.5 km from the crater. Layer B has a much higher proportion of lithics (red and gray) in all grain-size intervals compared to A-1, whereas layer C is intermediate between these two.

Bulk grain-size distributions of the three tephra-fall units have been determined at 6.5, 13, and 22 km from source. Beyond this distance, the three layers cannot be easily differentiated in the field and bulk grain-size analyses have been carried out on a combination of all three layers at 77, 137, and 173 km from source (Sigurdsson et al. 1984). Samples collected 6.5 km from source exhibit moderate to poor sorting with some

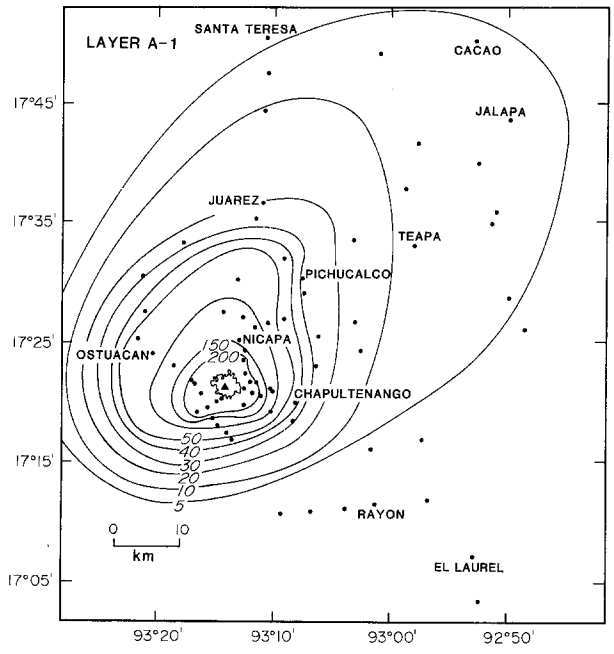

Fig. 5. Isopach map of layer A-1 from the March 29, 1982 eruption of El Chichon. Contour intervals in mm. Data collected during June 1982 and January 1983

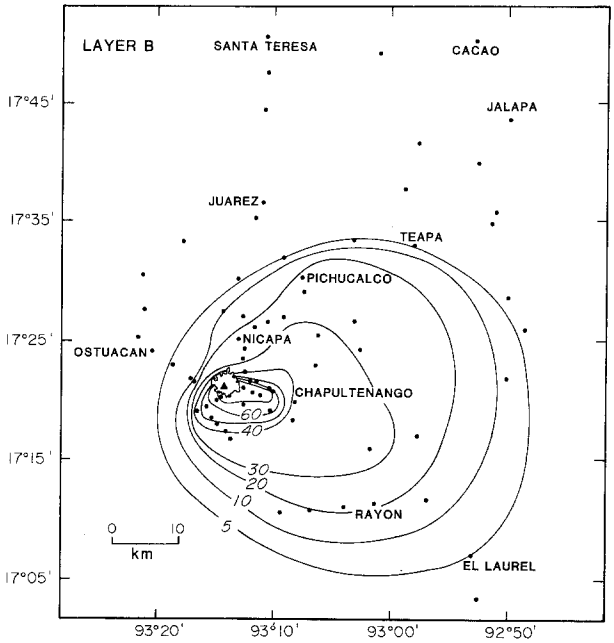

Fig. 6. Isopach map of layer B from the April 4 (0135 GMT), 1982 eruption of El Chichon. Contours in mm

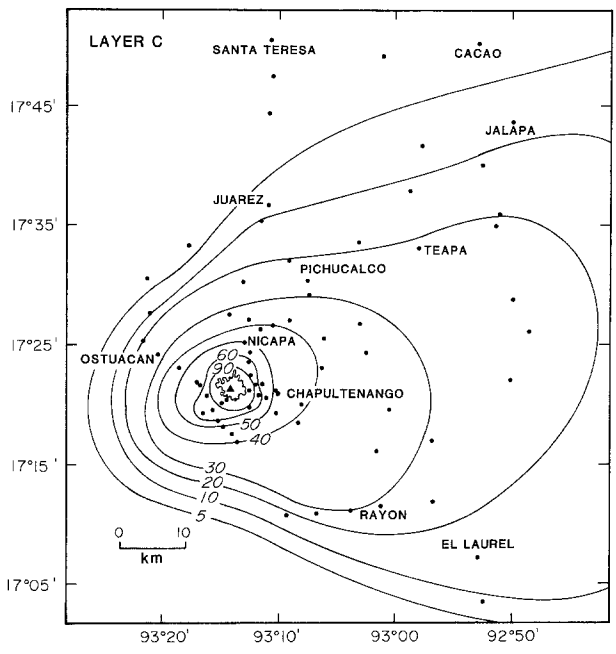

Fig. 7. Isopach map of layer C from the April 4 (1122 GMT), 1982 eruption of El Chichon. Contours in mm

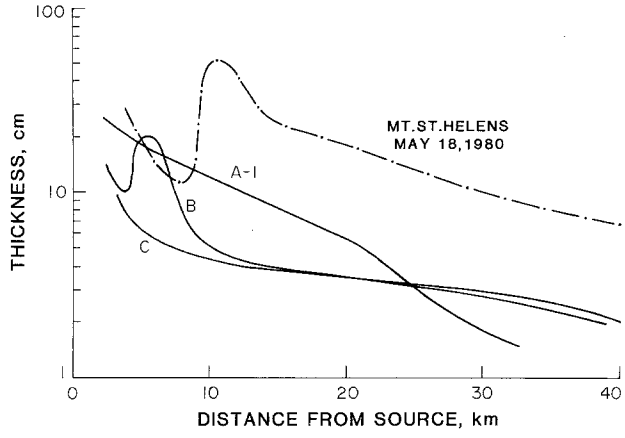

Fig. 8. Thickness versus distance from source for the A-1, B, and C tephra-fall layers. Note the secondary thickness maximum in the B layer and in the fall deposit from the May 18, 1980 eruption of Mount St. Helens (data from Waitt and Dzurisin 1981)

polymodality in the grain-size distribution that can be attributed to the hydraulic equivalency of an assemblage of variable density components (i.e., pumice, lithics, and crystals). Varekamp et al. (1984) cited a strong bimodality of the A-1 layer with modes at -1.5 and 3.0 phi at 17 km from source. This distribution results from combining the coarse base and fine top of layer A. We have subdivided their layer A into layers A-1 and A-2 and believe that they were derived from separate eruptions (Table 2; Sigurdsson et al. 1984). Polymodality is still, however, evident in our size distributions, and Varekamp et al. (1984) have made the important observation that particle aggregation is a

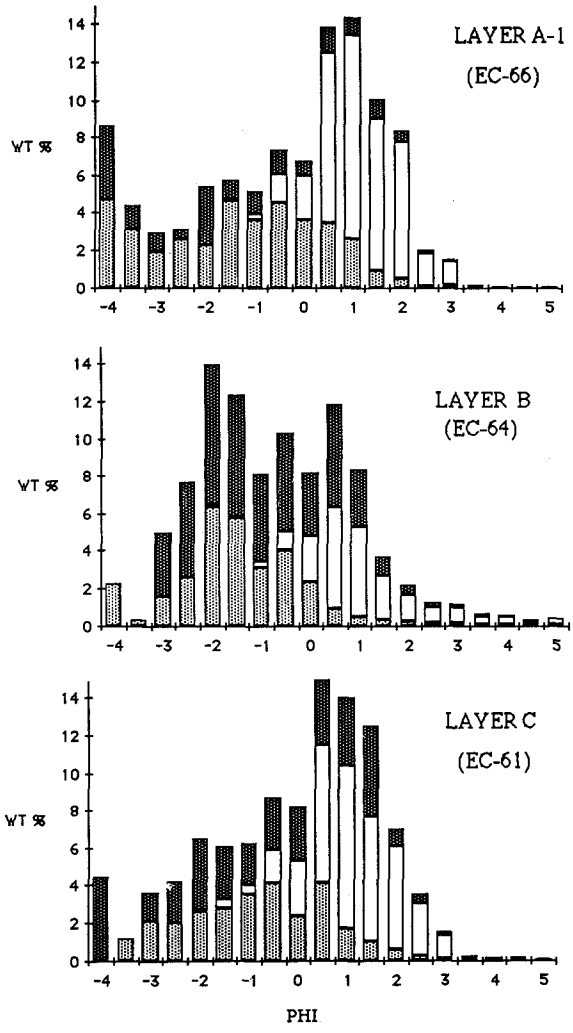

Fig. 9. Component abundances as a function of grain size for the A-1, B, and C tephra-fall layers. Dark-stippled pattern corresponds to lithics, light-stippled pattern to pumices, and white pattern to crystals. Fall layers were collected 6.5 km from source and are bulk samples

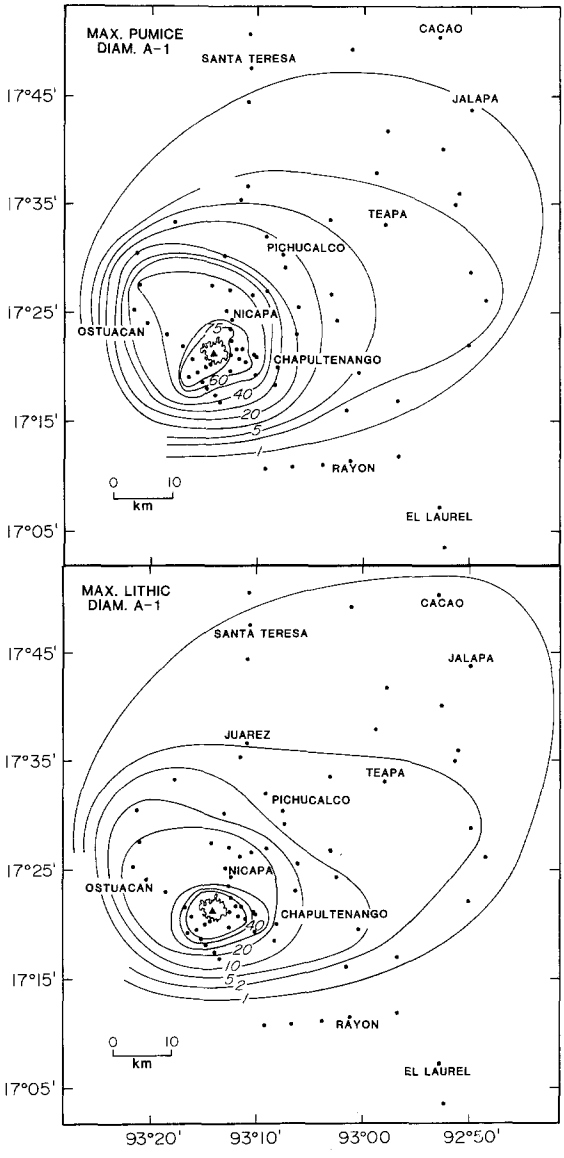

Fig. 10. Maximum pumice and lithic isopleths for the A-1 tephra-fall layer. Contours are in mm. Data are the average diameter of the five largest pyroclasts found in a 0.5 km^2 area through the entire layer

common feature in El Chichon tephra leading to coarse aggregate tails on the dry-sieved size distributions of distal samples. These "coarse tails" are not evident in our data set because our wet-sieving technique results in a breakup of the aggregates.

The average of the 5 largest pumices and lithics found in a standard cross section of each layer, 0.5 m^2 in area, were used to construct isopleth diagrams for the three fall deposits (Figs. 10–12). This technique provides a consistent method by which deposits from different eruptions can be compared. The data show that at a similar distance from source, layer B is significantly coarser, both in bulk grain size (Fig. 9) and maximum lithics (Fig. 13), than either layer A-1 or C. For example, at 5 km from the source, the maximum lithic size in layer B is twice that of either A or C. The grain size of layer C is slightly coarser than A-1, with few exceptions. The distribution of maximum pumices and lithics are used below to assess the eruption column dynamics and atmospheric transport of pyroclasts.

The grain-size data and isopach maps can be used to qualitatively assess differences in bulk fragmentation for each of the eruptions. As was pointed out above, layer B is distinctively coarser than either A-1 or C, yet it has the same thickness as layer C beyond 20 km from source. Layer A-1 is the thickest deposit close to the volcano, but becomes subordinate to layers B and C beyond 25 km from the source. These observations imply that layer B had the lowes-degree of fragmen-

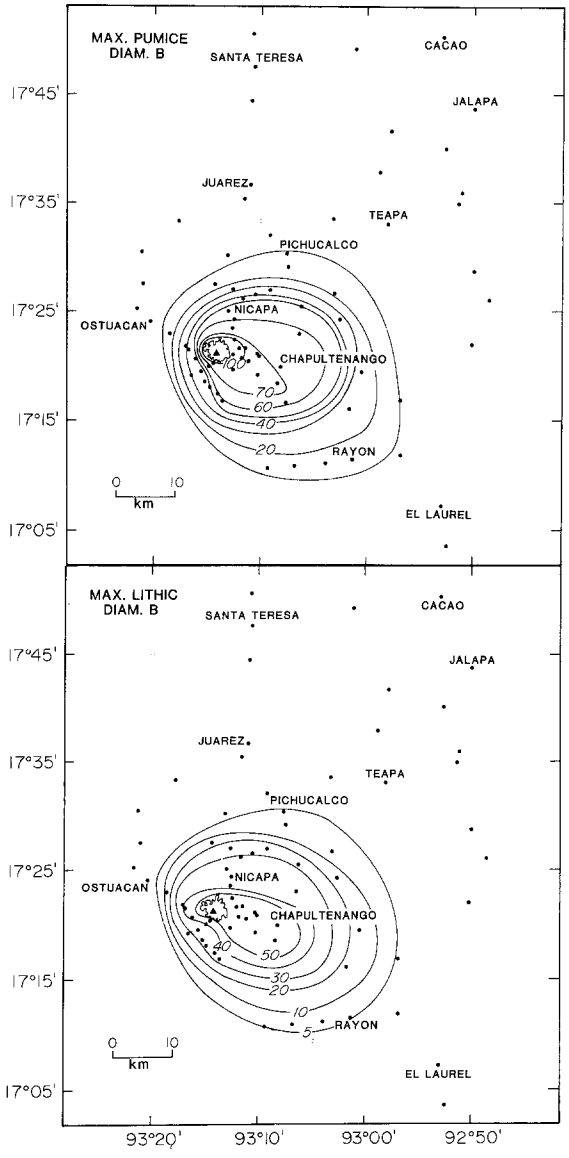

Fig. 11. Maximum pumice and lithic isopleths for the B tephra-fall layer. Contours are in mm

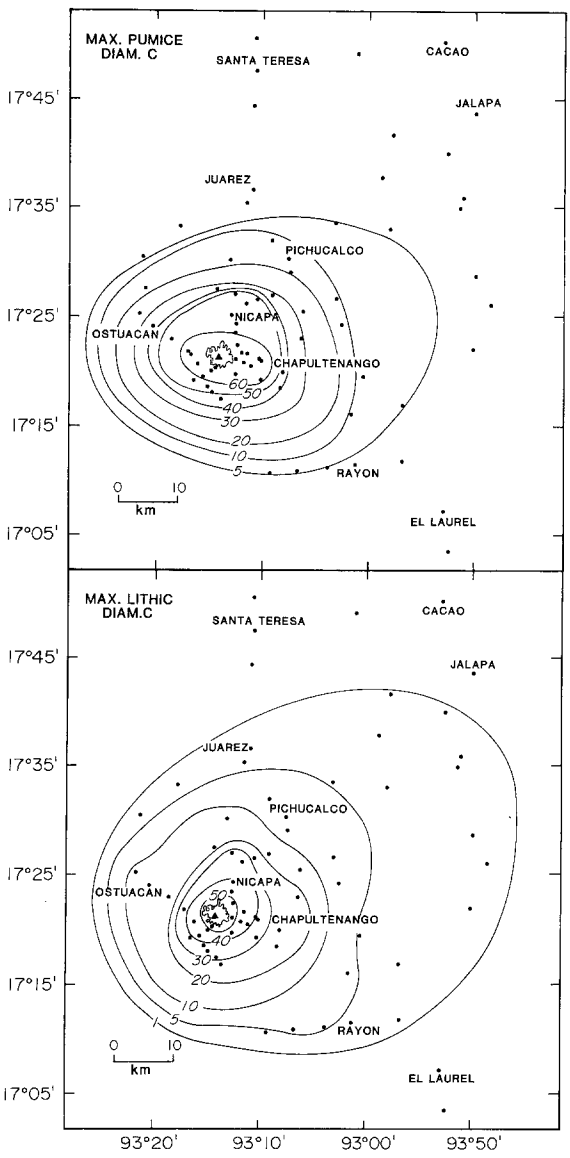

Fig. 12. Maximum pumice and lithic isopleths for the C tephra-fall layer. Contours are in mm

tation because it has a coarse proximal component and a moderate distal fine-ash component. In contrast, the highest degree of fragmentation is represented by layer C which has the largest distal fine-ash component. Intermediate between the two is layer A-1 which accumulated a large mass of material close to source with a relatively small volume of fine ash in the distal area.

Numerical modelling of pyroclast transport

The 1982 eruptions of El Chichon provide an opportunity to quantitatively examine the process of tephra dispersal from explosive eruptions as both meteorological data and field measurements of unmodified fall deposits are available. Such data sets are important tests and potential calibrations of tephra-dispersal models designed to reconstruct the dynamics and energetics of ancient explosive eruptions from the physical properties of pyroclastic deposits.

The principal factors which control the distribution of tephra from explosive eruptions are column height and wind speed. Carey and Sparks (1986) have developed a theoretical model for the fallout and dispersal of tephra which allows the role of column height and wind speed to be discriminated. The model is based on turbulent-plume theory (Morton et al. 1956) as mod-

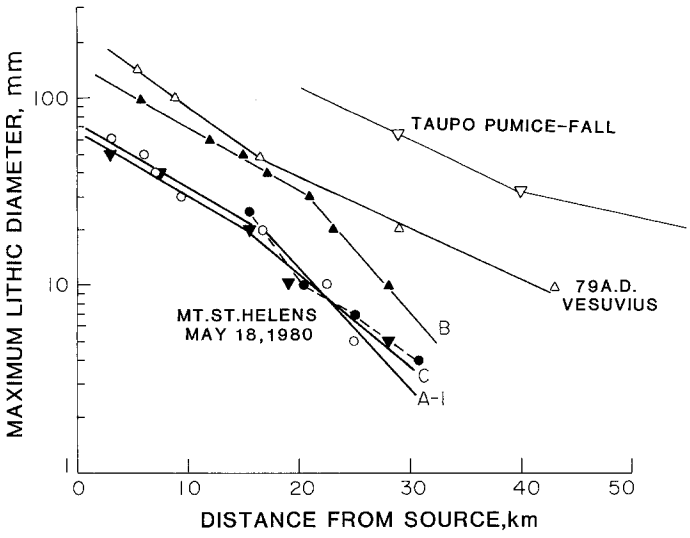

Fig. 13. Maximum average diameter of the five largest lithic clasts as a function of distance from source for the A-1 (open circles), B (solid triangles), and C (inverted solid triangles) El Chichon fall deposits. For comparison, data from the May 18, 1980 eruption of Mt. St. Helens (solid circles) (Carey and Sigurdsson, unpublished data), 79 A.D. eruption of Vesuvius (open triangles) (Sigurdsson et al. 1985), and the 1820 B.P. Taupo eruption (open inverted triangles) (Walker 1980) are also shown. Data are from transects along the main dispersal axis of each deposit

ified for volcanic eruptions (Wilson et al. 1978; Sparks and Wilson 1982; Sparks 1986). A numerical simulation of the model predicts the maximum distribution of a specific particle size as a function of column height for a given wind profile. By calculating the trajectories of three separate particles, the shape of the area of maximum distribution can be defined (Fig. 14). This area corresponds to a particle isopleth, which is routinely constructed from field data, and can be characterized by two parameters: the maximum half width measured perpendicular to the wind direction and the maximum downwind extent from the source (Fig. 14). The half width is strongly correlated with column height, as first suggested by Wilson (1978), whereas the downwind extent depends on both column height and wind speed. As a result, the geometry of particle isopleths can be used to estimate both column height and wind speed (Fig. 15).

Original calculations based on the theoretical model assumed a wind profile that was unidirectional at all altitudes as in Fig. 14 (Carey and Sparks 1986). In the case of the El Chichon eruptions, however, the main tropospheric and stratospheric transport were roughly in opposite directions (Fig. 2). A new set of calculations have been completed using a simplified wind profile that incorporates the reversal of transport directions (Fig. 16). The effect of the reversal is to decrease the maximum downwind dispersal of particles from eruption columns in excess of 21 km compared to the predictions based on the undirectional profile. This can be attributed to "back transport" within the stratosphere before particles settle below the tropopause.

Isopleth data for the A-1, B, and C eruptions generally fall close to the predicted trend for particle sizes of 0.8, 1.6, and 3.2 cm in diameter (Fig. 17). Eruption B tends to plot consistently on the downwind side of the predicted curve suggesting that the simplified wind profile may not be the best representation of the environmental conditions during this event. The data do indicate, however, that all of the eruptions produced columns which peaked above 25 km. Maximum column heights for the A-1, B, and C eruptions based on the average of the 0.8, 1.6, and 3.2 cm isopleths are 27.3, 31.6, and 28.8 km, respectively.

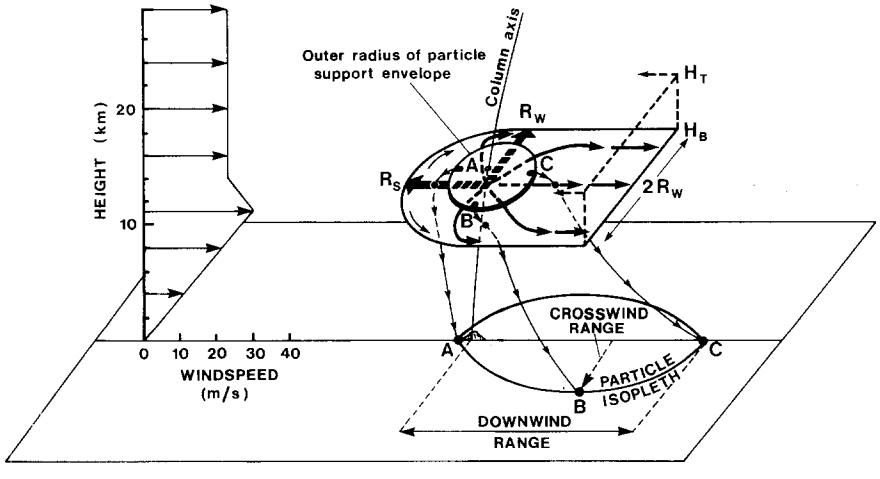

Fig. 14. Schematic representation of particle fallout from an eruption column in a crosswind. An upwind stagnation point develops at R_s where the radial velocity in the umbrella region (H_t–H_b) equals the crosswind velocity. Radial flow is deflected by the crosswind and passes through the downwind plane defined by H_t, H_b, and ZR_w Particles A (upwind), B (side), and C (downwind) are released from the outer radius of a particle support envelope determined by the locus of points where the average vertical velocity within the umbrella region is just equal to the terminal settling velocity of the particle. Trajectories of these three particles define the geometry of isopleth measured on the ground. Unidirectional wind profile is shown at left

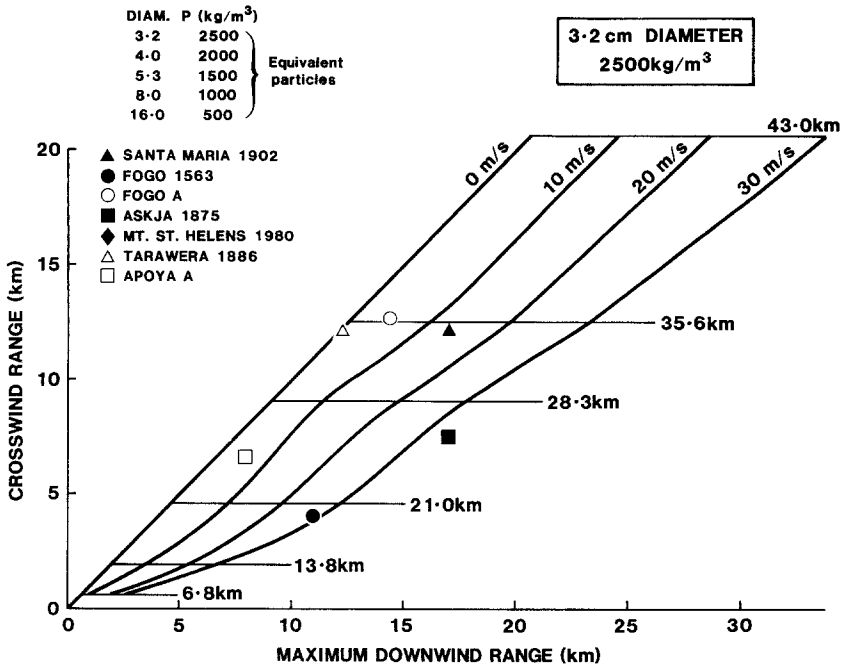

Fig. 15. Crosswind range versus maximum downwind range for a 0.8-cm-diameter lithic as calculated for eruption columns between 7 and 43 km height using a unidirectional wind profile (see Fig. 14) with maximum velocities of 10, 20, and 30 m/s. Equivalent particles are hydraulically equivalent combinations of particle density and diameter. A single particle isopleth defines a unique combination of column height and wind speed

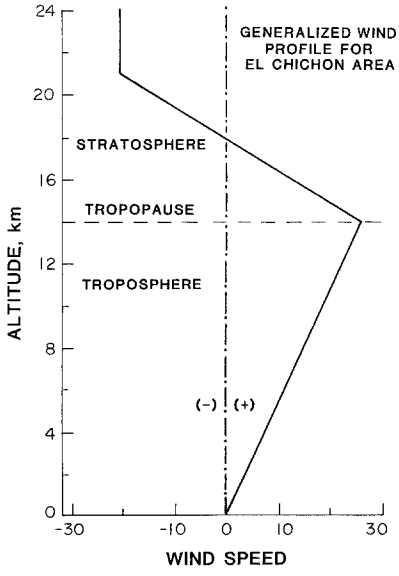

Fig. 16. Generalized wind profile for the El Chichon region compiled from radiosonde data at Merida, Veracruz, and Guatemala City. Negative wind speeds are directed 180° from positive values. Profile has been simplified to facilitate numerical modelling

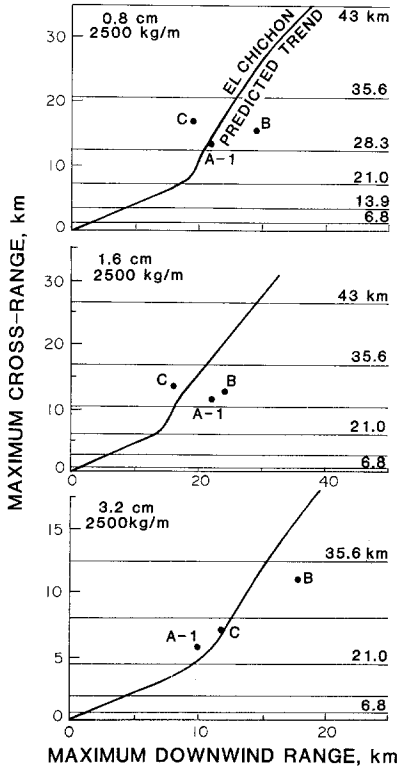

Fig. 17. Crosswind range versus maximum downwind range for 0.8-, 1.6-, and 3.2-cm-diameter lithic fragments as calculated for eruption column heights between 7 and 43 km using bidirectional wind profile (Fig. 16). Solid circles are acutal isopleth data for the A-1, B, and C eruptions. Inflections in the predicted curves results from "back transport" in the stratosphere for eruption column above 20 km

Tephra-fall volumes and mass eruption rates

Recent studies show that tephra volumes determined from the mappable portions of fall deposits are significantly underestimated due to distal fine-ash deposition beyond the mapped area (Walker 1980; Carey and Sigurdsson 1980; Rose et al. 1982). Two techniques are available to incorporate the distal fine-ash component: (1) integration of the function of isopach area versus thickness (Rose et al. 1973) and (2) mass balance based on the proportion of crystals versus melt in the magma (Walker 1980; Carey and Sigurdsson 1980). Walker (1981) has shown that for the Taupo pumice fall, integration to a minimum thickness of 1 micron is required to match the volume of tephra calculated by the crystal/glass fractionation method.

Gutierrez-Coutino et al. (1983) estimated the total volume of tephra fall from the three major eruptions of El Chichon to be 0.45 km^3 (DRE, dense rock equivalent) based on isopach data collected less than three weeks after the eruption (Table 3). These field data are regarded as most reliable as they were collected prior to compaction and erosion of the deposit by rainfall. Extapolation of this isopach data to the 1 micron thickness yields a total volume of 1.09 km^3 (DRE) (Table 3) or about 2 times the volume of the mappable deposit. By using the duration of each event and the equation relating column height to thermal flux (Wilson et al. 1978; Sparks and Wilson 1982):

$$H = 5.773\ (1+n)^{-3/8}\ [QsT]^{1/4}, \qquad (1)$$

where H is the column height in meters, n is the ratio of vertical gradient of absolute temperature to the adiabatic lapse rate, Q is the mass eruption rate, s is the specific heat of the tephra, and T is the temperature difference between the tephra and surrounding atmosphere, it is possible to calculate column height for the discharge of a specific volume of tephra. A magmatic temperature of 850° C has been adopted for all thermal-flux calculations (Luhr et al. 1984). If we first assume that the volume mapped on the ground represents total erupted volume, then the average column heights for the A-1, B, and C eruptions would be 16, 20, and 17 km, respectively. On the other hand, the extrapolated volumes would indicate average column heights of 20, 24, and 22 km, respectively.

Evidence of maximum column height in excess of 25 km for each eruption is provided by the numerical modelling of pyroclast dispersal and the presence of a stratospheric aerosol layer up to 30 km (Hofmann and Rosen 1983). Normal grading in the deposits suggests, however, that maximum column heights occurred at the onset of each event and then diminished with time. A complete reconstruction of the temporal evolution of column height would require detailed measurements of particle size as a function of stratigraphic height in the fall deposits, but the low thickness of the deposits preclude such analysis. Some insight into the relative change in column height during the events can, however, be obtained from remote-sensing observations. Satellite images of the three eruptions show a dense WSW stratospheric plume being generated throughout most of each event. There is no evidence of early detachment of the stratospheric plume as might be expected if the column height diminished rapidly to an altitude below the tropopause. Further evidence for sustained stratospheric plumes comes from the aerosol layer produced by the 1982 activity (McCormick et al. 1984). Maximum backscatter ratios measured by lidar 3 months after the eruptions were between 25 and 30 km, with a smaller subsidary peak between 22 and 24 km. Similarly, ballonborne measurements of particle con-

Table 3. 1982 El Chicon tephra-fall volumes

Eruption	Vol. (km^3)[a]	(DRE)[b]	Vol. (km^3)[c]	(DRE)[d]	MER[e]	Col. H_t (km)[f]
March 29 A-1 (0532 GMT)	0.19	0.10	0.60	0.30	3.5×10^7	20
April 4 B (0135 GMT)	0.36	0.19	0.79	0.39	6.0×10^7	24
April 4 C (1122 GMT)	0.31	0.16	0.80	0.40	4.0×10^7	22
Total	0.86	0.45	2.19	1.09		

[a] Volume of fall deposits mapped on the ground 3 weeks after the eruptions, Gutierrez-Coutino et al. (1983)
[b] Dense rock equivalent of (1) based on tephra density of 1.3 g/cm^3 and magma density of 2.5 g/cm^3
[c] Volume of fall deposits extrapolated to 1 micron thickness using the method of Rose et al. (1973)
[d] Dense rock equivalent of (3) based of tephra density of 1.3 g/cm^3 and a magma density of 2.5 g/cm^3
[e] Mass eruption rate (kg/s) calculated from extrapolated fall volumes (3) and durations estimated from satellite imagery (Table 2)
[f] Average column heights calculated using eq. (1) and average mass eruption rates (4)

centration revealed two major stratospheric layers, one centered at 25 km and the other at 21 km (Hofmann and Rosen 1983). It is likely that the altitude of aerosol maxima reflects the level at which sustained input of material occurred. Based on these observations we infer that eruption columns from the three events sustained for a significant portion of their duration at altitudes in excess of 22 km. Such altitudes are more in line with average column heights calculated from extrapolated tephra volumes and thus suggests that about half of the tephra fall was carried beyond the mapped deposit.

Maximum mass eruption rates calculated from Eq. (1) and column heights determined from the numerical modelling of pyroclast distribution are 1.1×10^8, 1.9×10^8, and 1.3×10^8 kg/s for the A-1, B, and C eruptions, respectively. Based on the presence of normal grading in the fall deposits, we infer that these rates apply only to the beginning of each eruption. Average mass eruption rates calculated from the total duration and volume of tephra produced by each event are shown in Table 3.

Discussion

Satellite images of plumes from the three major explosive eruptions of El Chichon together with meterological data demonstrate that tephra was distributed in two directions as a result of a major wind reversal above the tropopause. The orientation of the fallout axis and asymmetry of isopach contours for each layer indicates that deposition occurred primarily from plumes transported east-northeast in the tropopause. The ash transported in the stratosphere was apparently so fine grained that it settled out only after very wide dispersal of the plume over the Pacific Ocean. Of the three deposits, layer B is the least fragmented and contains the largest amount of lithics. These characteristics are the result of extensive erosion and disruption of the old summit dome through which the vent system penetrated (Sigurdsson et al. 1984).

Each of the eruption columns penetrated the tropopause and generated strong gravity waves (Mauk 1983). Based on considerations of tephra volumes, eruption durations, and transport directions we infer that column heights were sustained for some time at an altitude of at least 22 km for all of the major events. Matson (1984) cited column heights of 18.5, 16.9, and 16.9 km for certain periods of the A-1, B, and C eruptions, respectively, based on the correspondence between infrared-derived plume temperatures and radiosonde profiles at Veracruz. Column heights were assessed using the lowest plume temperatures, but as a result of the temperature reversal at the tropopause, a unique assignment of altitude is not possible. Eruption columns in the range 21–25 km would register temperatures warmer than those near the tropopause and thus choosing the minimum IR temperature would lead to an underestimate of the column height. Matson (1984) did, however, ascribe stratosperic heights of between 21 and 24 km to eruption plumes from the B and C eruptions based on transport directions and plume velocities.

In early May and late July 1982 the stratospheric cloud from the El Chichon eruptions was sampled between 16.8 and 19.2 km as part of the Dept. of Energy's Project Airstream (Mackinnon et al. 1984). The data collected on these missions provides important constraints on the heights attained by the 1982 eruption columns. Samples consisted mostly of angular glass shards with minor crystalline phases between 2 and 40 um in size. Many of the particles were in the form of clusters, some of which exceeded 50 um in size. Mackinnon et al. (1984) analyzed the particle-size data from the two missions using the settling velocity equations of Wilson and Huang (1979) and assuming eruption cloud heights of 26 km. The predicted sizes of particles at 18 km on the dates of the two missions are close to measured values, confirming column heights in excess of 25 km. Mackinnon et al. (1984) state, however, that the largest particles collected at 18 km were somewhat larger than the values predicted by the Wilson and Huang equations. This descrepancy may be due to a higher initial cloud top, i.e., >26 km. Our modelling of particle fallout from the El Chichon eruptions indicates that maximum column heights for the A-1, B, and C eruptions were 27.3, 31.6, and 28.8 km, respectively. Thus, the stratospheric particle-size data provides independent support for the results of the theoretical fallout model.

Normal grading in the three El Chichon fall layers suggests that eruption columns reached maximum elevation early in each event. A reduction in column height, i.e., in magma discharge rate, may have been the result of decreasing overpressure in the magma chamber and conduit system, a rearrangement in the geometry of the vent/conduit system, or a change in the rheological properties of the magma. Scandone and Malone (1985) have suggested that the relative difference between magma discharge rate at the surface (MDR) and magma supply rate from depth (MSR) controls the style of an explosive event. When MDR is close or equal to MSR, a sustained explosive eruption occurs such as the May 18, 1980 eruption of Mount St. Helens (Carey and Sigurdsson 1985). If MSR becomes less than MDR, an eruption tends toward a pulsatory style because the level of magma fragmentation migrates rapidly downward until fagmentation is eventually inhibited.

Scandone and Malone (1985) applied the model to explain the change in eruptive style at Mount St Helens

during 1980–1981. A systematic decrease in MSR at Mount St. Helens with time was attributed to an increase in magma viscosity as progressively more volatile-poor magma was being tapped. The magma at El Chichon was unusually crystal rich with up to 56 wt% phenocrysts and microphenocrysts (Luhr et al. 1984; Carey and Sigurdsson 1985). This high degree of crystallinity would result in a magma viscosity as high as 2.5×10^{10} poise (Mc Birney and Murase 1984; Shaw 1972), significantly greater than the magma erupted at Mount St. Helens on May 18, 1980 (Scandone and Malone 1985; Carey and Sigurdsson 1985). The rapid succession of relatively short eruptions at El Chichon, particularly in the period April 3–4, suggests that MSR was less than the MDR, and that the low MSR may reflect the crystal-rich and highly viscous nature of the magma.

Each event was probably preceded by a period during which overpressure developed either as a result of volatile exsolution or the density contrast between magma and crust. Once triggered, perhaps by a phreatomagmatic explosion, each event had a high initial magma discharge rate which then decreased as overpressures fell and the magma disruption level migrated downward. As a result, the fall deposits are relatively thin and normally graded. Most fall deposits will, of course, exhibit some normal grading as residual fine ash in the atmosphere settles out after an eruption ceases, but the lack of basal reverse grading, as observed, for example, in the 79 A.D. Vesuvius fall deposit (Lirer et al. 1973; Sigurdsson et al. 1985), supports the interpretation of high initial eruption columns.

The injection of tephra into the stratosphere by the El Chichon eruptions was also accompanied by a significant amount of sulfur, initially as gaseous SO_2. In the months following the eruptions the sulfur component of the stratospheric cloud underwent a gas to sulfuric acid-droplet conversion (Hofman and Rosen 1984a; Hofman and Rosen 1984b). Ballonborne measurements indicate that the total stratospheric aerosol mass may have been as much as 1.8×10^{13} g (Hofman and Rosen 1983; McCormick and Swissler 1983; Mroz et al. 1983). The sulfur-rich aerosol cloud showed two prominent peaks in particle concentration as a function of altitude. A lower peak was centered at about 21 km and an upper peak at 25 km (Hofman and Rosen 1983). Gradually, however, the two layers mixed and by the end of 1982 only a single broad peak, extending from the tropopause to about 30 km, was detected.

The origin of the two peaks, separated by a generally clean intermediate region, may be related to variations in mass discharge rate (i. e., column height) between the three El Chichon eruptions. One possibility is that the upper peak is associated with a particularly energetic eruption. We have shown based on satellite imagery and the distribution of maximum lithics that eruption B had the largest average mass eruption rate of the three events and therefore may have been responsible for the 25-km aeorsol peak. In this scenario, the lower peak would be attributed to a combination of the A-1 and C eruptions. Alternatively, the numerical simulations of tephra fallout suggest that all three eruptions had maximum column heights above 25 km at least temporarily during each event. We do not have enough data to reconstruct the entire history of each eruption column as the layers are thin, and only the maximum particle size within each fall layer was measured in the field. If the maximum column heights were discrete pulses relative to some stable, average discharge, then the upper peak could be interpreted as the cumulative effect of the maximum discharges for all three eruptions, whereas the lower peak represents the cumulative effect of the average discharge during the events. We prefer the latter interpretation at this time primarily because of the results from the numerical simulations of tephra fallout.

Conclusions

Three widespread tephra-fall deposits were formed by the March 29 (0532 UT, A-1), April 4 (0135 UT, B), and April 4 (1122 UT, C), 1982 explosive eruptions of El Chichon volcano in southeastern Mexico. Dispersal and grain-size characteristics of the layers indicate that the eruptions were moderate plinian events with some indication of phreatomagmatic activity. The rapid succession of these relatively short-lived eruptions may have been controlled by a relatively low rate of magma supply at depth compared to the rate of magma discharge at the surface. Each event generated an eruption column which penetrated the tropopause and was sheared in two directions by a reversal in wind direction between 18 and 20 km. A numerical simulation of tephra fallout used in conjunction with field data on the maximum dispersal of lithic fragments indicates maximum eruption column heights of 27.3, 31.6, and 28.8 km for the A-1, B, and C eruptions, respectively. These correspond to maximum magma discharge rates of 1.1×10^8, 1.9×10^8, and 1.3×10^8 kg/s. Normal grading in the fall deposits indicates that maximum column heights occurred at or near the beginning of each event.

Two stratospheric peaks in sulfur-aerosol concentration at 18 and 25 km height, observed shortly after the eruptions, may be related to the peak and average discharges for the three events or, alternatively, the upper peak may correlate with the more energetic B eruption. New estimates of tephra-fall volume which

take into account the widely dispersed fine-ash component increase our original value of 0.74 km^3 (0.37 DRE) to 2.19 km^3 (1.09 DRE) total for all three eruptions. Only about one-half of the total tephra fall is present in the mappable portion of the deposits.

Acknowledgements. We are greatful for the help of Juan-Manuel Espindola, Winton Cornell, Dick Fisher, and David Gardella during our two field trips to El Chichon. We would also like to thank Ignacio Galindo of the Insituto de Geofisica, Universidad Nacional Autonoma de Mexico, for providing logistical support and interest in our research. Steve Sparks and Steve Tait provided thorough reviews of the manuscript many helpful suggestions. This work was funded by grants from the National Science Foundation (EAR-82 05955) and the National Geographic Society (2566-82).

References

Carey SN, Sigurdsson H (1980) The Roseau ash: deep-sea tephra deposits from a major eruption on Dominica, Lesser Antilles. J Volcanol Geotherm Res 7: 67–86

Carey SN, Sigurdsson H (1985) The May 18, 1980 eruption of Mount St. Helens 2. Modelling of dynamics of the plinian phase. J Geophys Res 90: 2948–2958

Carey S, Sparks RSJ (1986) Quantitative models of the fallout and dispersal of tephra-fall from volcanic eruption columns. Bull Volcanol 48: 109-125

Devine J, Sigurdsson H, Davis A, Self S, (1984) Estimates of sulfur and chlorine yield to the atmosphere from volcanic eruptions and potential climatic effects. J Geophys Res 89: 6309–6325

Duffield W, Tilling R, Canul R (1984) Geology of El Chichon volcano, Chiapas, Mexico. J Volcanol Geotherm Res 20: 117–132

Gutierrez-Coutino R, Moreno-Corzo M, Cruz-Borraz C (1983) Determination del volumen del material arrojado y grado de explosividad alcanyado por el Volcan Chichonal, Estado de Chiapas. In: El Volcan Chichonal (Proceedings of symposium during the convention of Geological Society of Mexico). Insituto de Geologia, Universidad Nacional Autonoma

Havskov J, De la Cruz-Reyna S, Singh S, Medina F, Gutierrez C (1983) Seismic activity related to the March-April 1982 eruptions of El Chinon volcano, Chiapas, Mexico. Geophys Res Lett 10: 293–296

Hofman D, Rosen J (1983) Stratospheric sulfuric acid fraction and mass estimate for the 1982 volcanic eruption of El Chichon. Geophys Res Lett 10: 313–316

Hofman D, Rosen J (1984a) On the temporal variation of stratospheric aerosol size and mass during the first 18 months following the 1982 eruptions of El Chichon. J Geophys Res 89: 4883–4890

Hofman D, Rosen J, (1984b) Ballonborne particle counter observations of the El Chichon aerosol layers in the 0.01–1.8 um radius range. Geofis Int 23: 155–186

Krueger A (1982) Geostationary satellite observations of the April 1979 Soufriere eruptions. Science 216: 1108–1109

Lirer L, Pescatore T, Booth B, Walker G (1973) Two plinian pumice-fall deposits from Somma-Vesuvius, Italy. Geol Soc Am Bull 84: 759–772

Luhr J, Carmichael ISE, Varekamp J (1984) The 1982 eruptions of El Chichon volcano, Chiapas, Mexico: mineralogy and petrology of the anhydrite-bearing pumices. J Volcanol Geotherm Res 23: 69–108

Luther F, MacCracken M (1982) Radiative and climatic effects of the El Chichon eruption. EOS, Trans Am Geophys Union 63: 902

Mackinnon I, Gooding J, McKay D, Clanton U (1984) The El Chichon stratospheric cloud: solid particulates and settling rates. J Volcanol Geotherm Res 23: 125–146

Matson M (1984) The 1982 El Chichon volcano eruptions – a satellite perspective. J Volcanol Geotherm Res 23: 1–10

Mauk FJ (1983) Utilization of seismicity recorded infrasonic-acoustic signals to monitor volcanic explosion; the El Chichon sequence 1982, a case study. J. Geophys Res 88: 10385–10401

McBirney A, Murase T (1984) Rheological properties of magmas. Ann Rev Earth Planet Sci 12: 337–357

McCormick MP, Swissler T (1983) Stratospheric aerosol mass and latitudinal distribution of the El Chichon eruption cloud for October 1982. Geophys Res Lett 10: 877–880

McCormick MP, Swissler TJ, Fuller WH, Hunt WH, Osborn MT (1984) Airborne and ground-based lidar measurements of the El Chichon stratospheric aerosol from 90 N to 56 S. Geofis Int 23–2: 187–221

Morton B, Taylor G, Turner JS (1956) Turbulent gravitational convection from maintained and instantaneous sources. Proc R Soc London A234: 1–23

Mroz E, Mason A, Sedlacek W (1983) Stratospheric sulfate from El Chichon and the mystery volcano. Geophys Res Lett 10: 873–876

National Earth Satellite Service (Ness) (1982) El Chichon volcanic eruptions (WAB467, 10 minute silent film). Walter Boham Co, Washington, DC

Pollak J, Ackerman T, Toon OB (1982) Influence of the El Chichon cloud on the erarth's radiative balance. EOS, Trans Am Geophys Union 63: 902

Rampino M, Self S (1982) Historic eruptions of Tambora (1815) and Agung (1963), stratospheric aerosols, and climatic impact. Quat Res 18: 127–143

Rose WI, Bonis S, Stoiber R, Keller H, Bickford T (1973) Studies of volcanic ash from two recent Central American eruptions. Bull Volcanol 37: 338–363

Rose WI, Harris DM, Heiken G, Sarna-Wojcicki A, Self S (1982) Volcanological description of the 18 May, 1980, eruptions of Mount St. Helens NASA SP-458: 1–36

Rose WI, Wunderman R, Hoffman M, Gale L (1983) A volcanologists's review of atmospheric hazards of volcanic activity: Fuego and Mount St. Helens. J Volcanol Geotherm Res 17: 133–157

Rye R, Luhr J, Wasserman M (1984) Sulfur and oxygen isotopic systematics of the 1982 eruptions of El Chichon volcano, Chiapas, Mexico. J Volcanol Geotherm Res 23: 109–123

Sarna-Wojcicki A, Shipley S, Waitt R, Dzurisin D, Wood S (1982) Areal distribution, thickness, mass, volume and grain size of air-fall ash from the six major eruptions of 1980. In: Lipman PW and Mullineaux DR (eds) The 1980 Eruptions of Mount St. Helens, Washington US Geol Surv Prof Pap 1250: 577–600

Scandone R, Malone S (1985) Magma supply, magma discharge, and readjustment of the feeding system of Mount St. Helens during 1980. J Volcanol Geotherm Res 23: 239–262

Sean (Scientific Event Alert Network) 1-3: 3-5

Self S, Sparks SRJ (1978) Characteristics of wide-spread pyroclastic deposits formed by the interaction of silicic magma and water. Bull Volcanol 41: 1–17

Shaw HR (1972) Viscosities of magmatic silicate liquids: an empirical method of prediction. Am J Sci 272: 870–893

Sigurdsson H, Carey S, Espindola JM, (1984) The 1982 eruptions of El Chichon, Mexico: stratigraphy of pyroclastic deposits. Volcanol Geotherm Res 23: 11–37

Sigurdsson H, Carey S, Cornell W, Pescatore T (1985) The eruption of Vesuvius in 79 A.D. National Geographic Research 1–3: 332–387

Sparks RSJ (1986) The dimensions and dynamics of volcanic eruption columns. Bull Volcanol 48: 3-15

Sparks RSJ, Wilson L (1982) Explosive volcanic eruptions – V.

observations of plume dynmics during the 1979 Soufriere eruption, St. Vincent. Geophys JR Astr Soc 69: 551–570

Sparks RSJ, Moore JG, Rice C (1986) The giant eruption cloud of the May 18, 1980, explosive eruption of Mount St. Helens. Bull Volcanol (in press).

Tilling RL, Rubin M, Sigurdsson H, Carey S, Duffield W, Rose W (1984) Prehistoric eruptive activity of El Chichon volcano, Mexico. Science 224: 747–749

Varekamp J, Luhr J, Prestegaard K (1984) The 1982 eruptions of El Chichon volcano (Chiapas, Mexico): character of the eruptions, ash-fall deposits and gas phase. J Volcanol Geotherm Res 23: 39–68

Waitt RB, Dzurisin D (1981) Proximal air-fall deposits from the May 18 eruption-stratigraphy and field sedimentology. In: Lipman PW, Mullineaux DR (eds) The 1980 Eruptions of Mount St. Helens, Washington US Geol Surv Pap 1250: 601–616

Walker GPL, (1980) The Taupo pumice: product of the most powerful known (ultraplinian) eruption. J Volcanol Geotherm Res 8: 69–94

Walker GPL (1981) Plinian eruptions and their products. Bull Volcanol 44: 223–240

Williams S, Self S (1983) The October 1902 pliniam eruption of Santa Maria volcano, Guatemala. J Volcanol Geotherm Res 16: 33–56

Wilson L (1978) Energetics of the Minoan eruption. In: C Doumas (ed) Thera and the Aegean world I.

Wilson L, Huang TC (1979) The influence of shape on the atmospheric settling velocity of volcanic ash particles. Earth Planet Scie Lett 44: 311–124

Wilson L, Sparks RSJ, Huang TC, Watkins ND (1978) The control of volcanic column eruption height by eruption energetics and dynamics. J Geophys Res 83: 1829–1836

Received September 2, 1985/Accepted November 15, 1985